Solar Phys (2007) 241: 385–396
DOI 10.1007/s11207-007-0276-9

Analysis of Solar Wind Events Using Interplanetary Scintillation Remote Sensing 3D Reconstructions and Their Comparison at Mars

B.V. Jackson · J.A. Boyer · P.P. Hick · A. Buffington · M.M. Bisi · D.H. Crider

Received: 22 July 2006 / Accepted: 16 January 2007 /
Published online: 4 April 2007

Abstract Interplanetary Scintillation (IPS) allows observation of the inner heliospheric response to corotating solar structures and coronal mass ejections (CMEs) in scintillation level and velocity. With colleagues at STELab, Nagoya University, Japan, we have developed near-real-time access of STELab IPS data for use in space-weather forecasting. We use a 3D reconstruction technique that produces perspective views from solar corotating plasma and outward-flowing solar wind as observed from Earth by iteratively fitting a kinematic solar wind model to IPS observations. This 3D modeling technique permits reconstruction of the density and velocity structure of CMEs and other interplanetary transients at a relatively coarse resolution: a solar rotational cadence and 10° latitudinal and longitudinal resolution for the corotational model and a one-day cadence and 20° latitudinal and longitudinal heliographic resolution for the time-dependent model. This technique is used to determine solar-wind pressure ("ram" pressure) at Mars. Results are compared with ram-pressure observations derived from *Mars Global Surveyor* magnetometer data (Crider *et al.*, 2003, *J. Geophys. Res.* **108**(A12), 1461) for the years 1999 through 2004. We identified 47 independent *in situ* pressure-pulse events above 3.5 nPa in the *Mars Global Surveyor* data in this time period where sufficient IPS data were available. We detail the large pressure pulse observed at Mars in association with a CME that erupted from the Sun on 27 May 2003, which was a halo CME as viewed from Earth. We also detail the response of a series of West-limb CME events and compare their response observed at Mars about 160° west of the Sun – Earth line by the *Mars Global Surveyor* with the response derived from the IPS 3D reconstructions.

B.V. Jackson (✉) · J.A. Boyer · P.P. Hick · A. Buffington · M.M. Bisi
Center for Astrophysics and Space Sciences, University of California, San Diego, CA 92093, USA
e-mail: bvjackson@ucsd.edu

D.H. Crider
Catholic University of America, Washington, DC 20064, USA

1. Introduction

Interplanetary scintillation (IPS) observations of meter-wavelength intensity variations from point radio sources are one source of heliospheric remote-sensing information. These have long been used to measure small-scale (∼200 km) density variations along the line of sight to a radio source (*e.g.,* Hewish, Scott, and Wills, 1964; Ananthakrishnan, Coles, and Kaufman, 1980). IPS observations taken using the Cambridge IPS array in the United Kingdom (Houminer, 1971) show structures that can be classified as either corotating or detached from the Sun (Gapper *et al.*, 1982; Hewish and Bravo, 1986; Behannon, Burlaga, and Hewish, 1991).

To optimize the use of IPS measurements and produce 3D global representations of the heliosphere from observations of point radio sources at specific locations in the sky covering a large range of elongations, we have developed a Computer Assisted Tomography (CAT) program (Jackson *et al.*, 1998, 2003; Jackson, Hick, and Buffington, 2002; Hick and Jackson, 2003; Jackson and Hick, 2004) that fits these data to a solar-wind model. We fit STELab (Nagoya University) IPS observations (Kojima and Kakinuma, 1987; Jackson and Hick, 2004) and have operated a real-time forecasting system during the nine-month period each year when the STELab scintillation arrays take data. Two models are used. The first model assumes that the heliosphere is unchanging except for outward solar-wind flow over intervals of one solar rotation (a corotating model). In this model, solar rotation provides the primary change in perspective view for each observed location. The second model is time-dependent, allowing time to vary with an interval (usually one day) that is short compared with that of a solar rotation. This short interval imposes the restriction that the reconstructions primarily use outward solar-wind motion to give perspective views of each point in space. The results to date are commensurate with, but also limited by, the observational coverage, temporal and spatial resolution, and signal-to-noise ratio available from the STELab data.

The *Mars Global Surveyor* magnetometer measurements of the Martian magnetosphere have provided a proxy for solar-wind dynamic pressure at Mars since 1997. For the period of this study from 1999 to 2004, no other instrument at Mars provided direct solar-wind density or velocity measurements. Although the *Mars Express* spacecraft, which arrived at Mars in 2004, is equipped with an Ion Mass Analyzer (IMA), it does not *routinely* determine solar-wind parameters, and thus *Mars Global Surveyor* observations serve as an essential and more continuous measurement to characterize the interaction of the solar wind with Mars.

Previous 3D model reconstructions of velocities and densities at Earth (Jackson, Hick, and Buffington, 2002; Jackson and Hick, 2004) have shown good accuracy in retrospective analyses and in forecasts. The present analysis extends this work to relative locations of the largest events observed at Mars. Here, STELab velocity and g-level (radio scintillation level relative to the nominal one at that elongation) data are used to determine an arrival time and strengths of these pressure events. This analysis highlights the front-side halo CME event of 27 May 2003 and a series of West-limb CME events observed in September 2002, when Mars was opposite the Sun from Earth.

The next section describes the tomographic program developed to fit the IPS data and the technique used to deduce Mars ram pressure from the *Mars Global Surveyor* magnetometer data. The third section compares amplitudes and timings of the tomographic model pressure peaks to the event peaks of larger than 3.5 nPa observed by the *Mars Global Surveyor*. The final section presents a summary and conclusions.

2. 3D Reconstructions

The present tomography technique reconstructs 3D corotating or time-dependent solar-wind velocity and density matrices by applying an inversion technique to the IPS data. In the solar corona, when structures do not evolve significantly (except for corotation) on a time scale of one solar rotation, rotation alone yields sufficient information for reconstruction of the quiet corona. The corotational model, which assumes that observations to the East and to the West of the Sun are the same (see Jackson *et al.*, 1998), can be applied in this situation.

We also use a time-dependent 3D tomographic model. When a transient structure such as a heliospheric response to a CME is observed across a large range of solar elongations, it is viewed from widely different directions. This changing perspective is exploited to reconstruct a 3D time-dependent solar-wind model.

Both the corotating and time-dependent analyses incorporate the fact that line-of-sight observations are dominated by contributions from material closest to the Sun, because more scattering occurs there. However, no explicit assumptions are made about the distribution of velocity and density along these lines of sight. The inversion process begins with an assumed set of initial boundary conditions for the solar-wind model at 15 solar radii. In the case of the time-dependent model these boundaries are set at a regular time cadence (usually at one-day intervals centered at local noon in Nagoya, Japan). In the initial stage, these lower boundaries (source surfaces) are populated with an unstructured approximation of mass and velocity at that distance from the Sun. Currently, the model propagates mass and velocity outward from this source surface to beyond Earth by using a purely kinematic model. The IPS observations are remotely sensed from as close to the Sun as 11.5° elongation and outward (the weak scattering regime at 327 MHz). Each line of sight is carried to as distant as 2 AU from Earth. The highest signal from the observations generally comes from the closest approach of the line of sight to the Sun, with that point being 1 AU in the solar direction and close to Earth beyond about 60° elongation. At the ends of the lines of sight, signals from solar-wind observations are less than 5% of the average total values. The 3D model is formed out to at least 3 AU from the Sun, well beyond the orbit of Mars. The model assumes outward radial flow and enforces conservation of mass and mass flux (Jackson *et al.*, 1998; Jackson and Hick, 2004). Given the initial velocities and densities on the inner boundaries, a fully 3D solar-wind model over time is propagated throughout the inner heliosphere.

Line-of-sight IPS levels and velocities are generated from the solar-wind reconstructions that correspond to the specified weighting function for the frequency of the IPS data used (which for STELab observations is 327 MHz). The differences between observed and modeled quantities are projected back onto the source surface, by tracing each solar-wind packet within the 3D model back to its origin on the source surface. The differences between the observed and model data are used to update the initial mass and velocity distribution on the source surface boundary (or boundaries in the case of the time-dependent reconstruction). The tomographic inversion takes place on the inner boundary by iteratively fitting the model to the observations until a least-squares minimum of observations to the model is obtained. When the model does not reproduce the solar wind at large solar distances accurately enough, the source surface values are altered to improve the fit. Convergence is assumed when differences no longer change by more than a few percent. This usually occurs well within the maximum allowed 18 iterations.

Since only a few thousand lines of sight exist in any one given solar rotation, the resolution is determined by a set of Gaussian filters having a 10° × 10° latitude and longitude resolution for the corotating model and a 20° × 20° latitude and longitude resolution with a one-day temporal cadence for the time-dependent model. This resolution is good enough to determine the large-scale structure of solar-wind velocity and density. Tests show that after a few iterations, any specific residual of the initial boundary conditions is erased. The technique has been used successfully to analyze corotating solar-wind structures (Jackson *et al.*, 1998) and CME-associated velocity and density structures using both IPS and Thomson-scattering observations (Jackson and Hick, 2004; Jackson *et al.*, 2006), and these compare favorably with other techniques used to invert the IPS data (Tokumaru *et al.*, 2005, 2007).

Once the 3D solar-wind density and velocity have been calculated, time series at the position of Mars are extracted (interpolated in 3D in the case of the corotating model and in 4D in the case of the time-dependent model). A ram pressure (P) is derived from these by the equation

$$P = mnV^2 = 2 \times 10^{-6} nV^2. \tag{1}$$

The effective mass per electron (m) is taken to be 2.0 $\times 10^{-24}$ g; P is in nPa, n is in electrons cm^{-3}, and V is in $\mathrm{km\,s}^{-1}$. Several assumptions determine the accuracy of this conversion. The density derived from the tomography is calibrated by assuming a conversion from g-level small-scale electron-density fluctuations to density using a set of power-law relationships (Jackson *et al.*, 1998), in this case assumed to fit the Earth *in situ* proton-density measurements from the ACE spacecraft for the density peak associated with the 14 July 2000 (Bastille Day) CME (Jackson *et al.*, 2003). As in this event, a background density of 5 electrons cm^{-3} at 1 AU was assumed. In addition, in determining the effective mass per electron (m) a 10% helium abundance in the solar wind is assumed (Hildner *et al.*, 1975).

To compare the above values with *in situ* solar-wind measurements at Mars, the *Mars Global Surveyor* magnetometer measurements provide a proxy for solar-wind dynamic pressure at Mars by measuring the Martian magnetosphere magnetic-field magnitude (Vennerstrom *et al.*, 2003; Crider *et al.*, 2003). Since the Martian magnetosphere pressure only approximately balances the solar-wind dynamic pressure, it is important to find other ways to confirm these determinations at Mars.

Determination of the solar-wind ram pressure from the *Mars Global Surveyor* data is not entirely straightforward. First, magnetic-field measurements need to be selected distant from known Martian crustal sources of magnetic field. The technique further assumes that the contribution from Martian atmospheric gas pressure effects is small, and this includes thermal effects within the magnetic-pileup boundary. Magnetic pressure relative to the Martian surface is assumed to fall off relative to the angle of the incident solar-wind flow relative to the surface normal. Mapped during quiet times at Mars, these magnetic pressures form a curve fit to the location of the spacecraft relative to the solar zenith angle, and these relate to the pressure at the angle of incidence of solar-wind flow (Vennerstrom *et al.*, 2003). The analyses give good measurements of changes from one orbit pass to the next of the instrument through the pileup region of the Martian magnetosphere with an approximate time cadence of the orbital period of *Mars Global Surveyor*. Starting in March 1999, this period is a little under two hours. The period decreased from 44 hours to 2 hours from orbital insertion in September 1997 through March 1999. Absolute solar-wind pressures at Mars are derived from the knowledge of the magnetic-field pressure extrapolated to the stagnation point between the solar wind at the solar zenith even though the *Mars Global Surveyor* does not traverse this stagnation point. Consistency checks up to now have been provided by extrapolations from Earth to the vicinity of Mars over the period from 2 October 1997 to 31 December 1998 (Crider *et al.*, 2003) with additional checks at times of large events (*e.g.*, Crider *et al.*, 2005). This proxy is consistent with those used by Verigin *et al.* (2004), who allow the obstacle shape to vary, and by Brain *et al.* (2005), who include a variable gas pressure.

3. IPS Comparison with Mars Ram Pressure

We compare data gathered between 26 April 1999 and 7 December 2004, when both the STELab IPS arrays and *Mars Global Surveyor* were taking data. *Mars Global Surveyor* events above 3.5 nPa have pressures $>1.5\sigma$ above the center of a Gaussian fit to the log of the solar-wind pressure. To compare with peaks in the IPS reconstructions smoothed by Gaussian filters both spatially and in time, the *Mars Global Surveyor* data were smoothed using a one-day "boxcar" filter, and then independent peaks of more than 3.5 nPa were selected to be compared with peaks in the IPS data. *Mars Global Surveyor* data were examined within ± 3 days of the event peak time with the IPS data. In all, there were some 47 events above 3.5 nPa present in the *Mars Global Surveyor* data when the IPS arrays were operating, of which 20 were above 5 nPa and 5 were above 10 nPa. Of these 47 events, 42 were associated with peaks in the corotating analysis and 37 were associated with peaks in the time-dependent analysis. To determine whether an event on Mars was matched with an IPS event, several additional factors were considered, including the event's proximity to surrounding events, the shape and relative levels of the nearby IPS model peak values, and the relative value of the *Mars Global Surveyor* data peak above the local noise level.

The very largest events observed in the *Mars Global Surveyor* analyses have obvious solar manifestations associated with CMEs, including the 2003 Halloween solar "superstorms" observed during the end of October and early November (Crider *et al.*, 2005). We have studied the 28 October 2003 event in detail using both the Solar Mass Ejection Imager (SMEI) (see Eyles *et al.*, 2003; Jackson *et al.*, 2005), and with 3D density reconstructions in conjunction with IPS velocity data (Jackson *et al.*, 2006). We include this event in this study because it shows a huge response in the IPS reconstruction and in the *Mars Global Surveyor* data with a peak that lags the IPS time-dependent 3D reconstruction peak by about one day. Even so, we note that this event is anomalous and worthy of a more lengthy discussion, because of its very high speed and solar-surface manifestations and its differing responses from each spacecraft observing it near Earth. Otherwise, to characterize this study of many events throughout the time period of interest we have chosen several events observed at Mars: one is a "front-side" halo CME observed at the Sun on 27 May 2003, when Mars was in the hemisphere of the Sun toward Earth, and the others are a series of mostly West-limb CMEs observed in September 2002 when Mars was in the hemisphere away from Earth.

A remote view of the IPS-derived density for the first event from the time-dependent model is shown in Figure 1a. This view shows the approximate shape of the density structure associated with this CME. Figure 1b shows the relative locations of Earth and Mars at the time of the CME event. Figure 2 compares the *Mars Global Surveyor* ram-pressure time series with both the time-dependent and the corotating model. The halo CME of 27 May 2003 shows as a peak in the ram pressure beginning on 30 May 2003. The ram-pressure peak in the *Mars Global Surveyor* analysis is one of the highest seen among the events, with a value far above the minimum 3.5 nPa threshold imposed here. The comparison with the time-dependent model (Figure 2b) is observed well in the time-dependent 3D reconstructions, and perhaps is evident as a small delayed peak in the corotating analysis of Figure 2a.

Figures 3 and 4 show the equivalent to Figures 1 and 2, but for the series of CMEs, the beginning of which reach Mars on about 16 September 2002. The peaks in the ram pressure for these events agree fairly well in the comparison with the time-dependent tomography analysis. This ram-pressure event height reached a peak of about 3.8 nPa in the *Mars Global Surveyor* analysis at Mars, only slightly above the 3.5 value required for event comparison with the modeling. The only peak in the *Mars Global Surveyor* pressure analysis above the 3.5 nPa criterion during this interval occurred on 17 September 2002. As shown in the

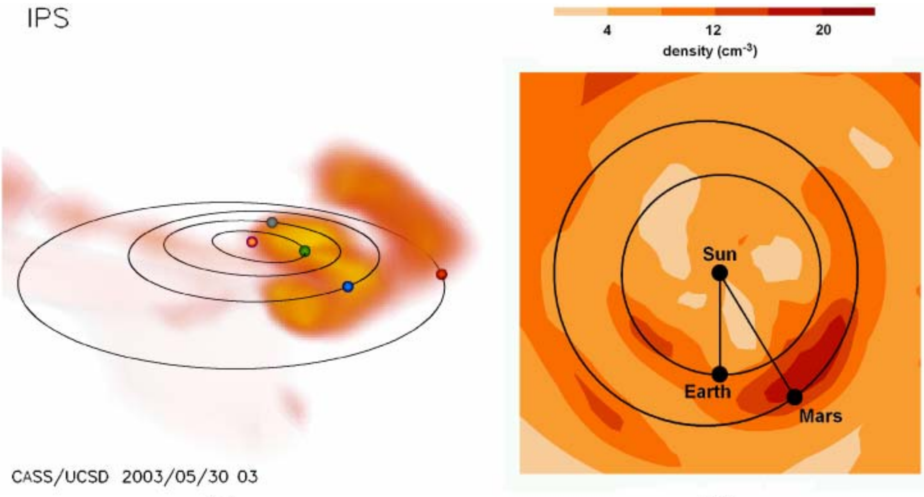

(a) **(b)**

Figure 1 (a) Remote observer view of the reconstructed density for the halo CME event of 27 May 2003. The view is from 30° above the ecliptic and about 30° east of the Sun – Earth line. Earth is the blue dot with its orbit shown as an ellipse beyond the orbits of Mercury and Venus. Mars is about to be engulfed by the CME. Electron density is scaled from 10 to 30 e^{-} cm^{-3} with an r^{-2} radial falloff removed by the analysis. (b) The relative locations of Earth and Mars at this time as seen from directly above the ecliptic plane, superimposed on the in-ecliptic density extracted from the tomographic reconstruction, also scaled as in (a).

reconstruction, the major portion of the CME mass passed between the Earth and Mars. Although the peak shown in the modeling is not as clear or as dominant as in the front-side halo event of Figures 1 and 2, there is nonetheless a peak that also appears in the response shown in both the time-dependent and corotating models. Since the IPS observations go no closer to the Sun than 11.5° elongation, the derivation of IPS model ram pressures at Mars across the gap closer than this behind the Sun are determined from measurements made at locations on either side of it. This type of comparison was carried out for all of the original 47 *Mars Global Surveyor* ram-pressure events above 3.5 nPa, regardless of their position with respect to the Sun – Earth line.

The ram-pressure events observed by the *Mars Global Surveyor* are shown in a series of scatter plots and histograms detailing the amplitudes and correlation comparisons of these events with the 3D reconstructions from the IPS data. Figures 5a and b show the comparison in peak amplitude between the pressure events seen by the *Mars Global Surveyor* and the time-dependent and the corotating model, respectively.

Figures 6a to e show the results of comparing *Mars Global Surveyor* peak-pressure time-series values to IPS model peak values within three days of the *Mars Global Surveyor* peak. The time shifts in peak values were determined for the most dominant peak within this three-day period for both time series. These time lags were binned in one-day intervals, with negative shifts indicating that the IPS model peak values precede the peak in the *Mars Global Surveyor* ram-pressure values. Conversely, positive shifts indicate the IPS model peak is late compared to the *Mars Surveyo*r peak. Of the 47 dominant peaks in the *Mars Global Surveyor* data, only those events were retained where a peak existed within the three-day interval in the IPS pressure model value time series. The background level shown in each histogram was determined by finding the distance in time to the next nearest peak of more than 3.5 nPa in the *Mars Global Surveyor* analysis for each event, summing these times in

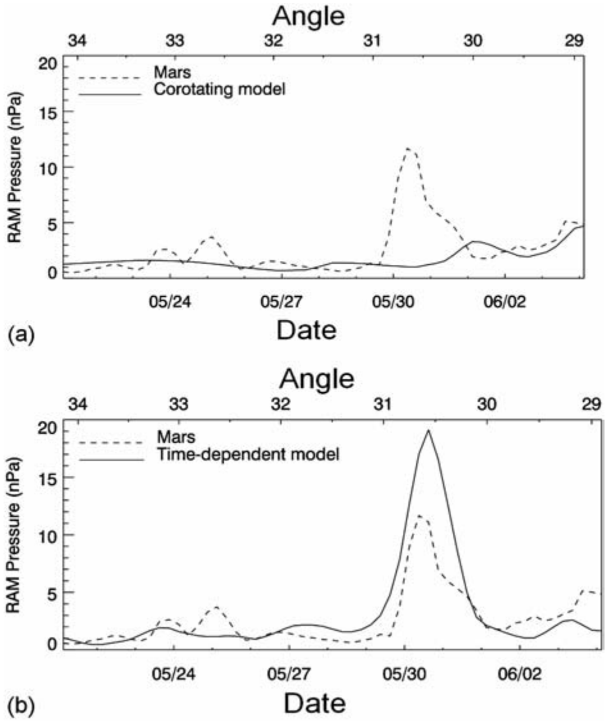

Figure 2 A comparison of IPS-derived ram pressure at Mars and *in situ* measurements derived from magnetic-field data for the time period from 21 May 2003 to 4 June 2003 covering the period of the 27 May 2003 CME event. The Mars *in situ* response to the event begins on 30 May 2003. The angle of Mars to the west of the Sun – Earth line is given at the top of each time series. (a) Corotating model. (b) Time-dependent model.

days, and then dividing the number of events by this sum. In other words, with ten events having an average of ten days to the next event, the occurrence rate number would be 1.0.

4. Summary and Conclusions

The 3D IPS solar-wind modeling clearly shows significant correlation in time with approximately the same amplitude when compared with the ram-pressure events observed at Mars by the *Mars Global Surveyor*. This correlation persists even when Mars is in the hemisphere on the opposite side of the Sun from the Earth. The modeling combines two IPS data sets, namely the IPS velocity data and the IPS g-level data that are used as a proxy for bulk solar-wind density. We expected the 3D solar-wind reconstructions to give satisfactory solar-wind values at Mars on some occasions, given the numerous good comparisons of the model at Earth with *in situ* spacecraft observations of both density and velocity (see Jackson *et al.*, 1998; Jackson and Hick, 2004; Dunn *et al.*, 2005), but this tests the combination of these nearly separate IPS velocity and density analyses. In addition, it tests this at a location other than the one used for the remote-sensing observations.

However, the details of the comparisons at Mars have some interesting features. Amplitude comparisons for both time-dependent and corotating events (Figures 5a and b) show only a weak correlation. Most of the events in the study are just above the Mars ram-pressure threshold of 3.5 nPa, with only a few events significantly above this relatively low threshold (a 1.5σ measurement in the *Mars Global Surveyor* analyses). There is a tendency for the IPS modeling to give lower values for the event peaks. The average IPS model ram-pressure

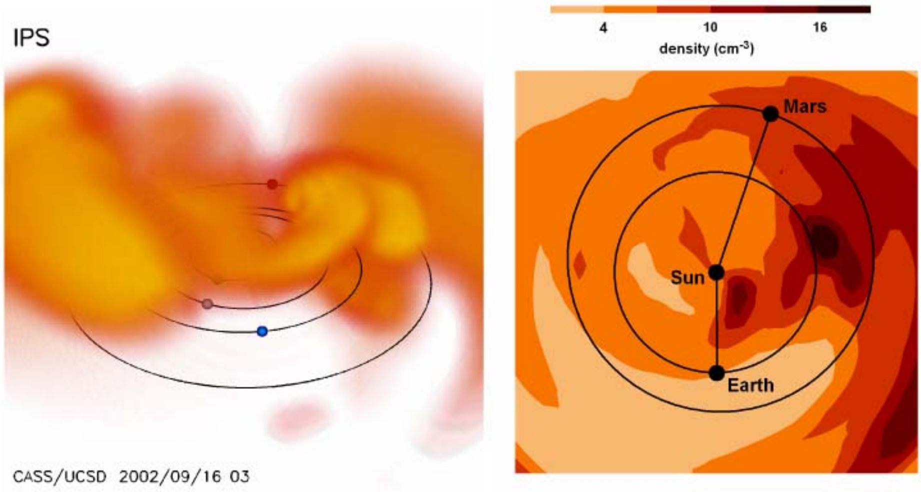

(a) (b)

Figure 3 (a) Remote observer view of the reconstructed density model associated with a series of West-limb CME events as observed on 0300 UT 16 September 2002. Earlier CMEs to the solar northeast were also present. The view is from 30° above the ecliptic and about 5° to the east of the Sun – Earth line. Earth is shown as a blue dot on its orbit beyond the orbits of Mercury and Venus. Mars is shown as a dot on its orbit in the distance. Electron density is scaled from 5 to 15 e^{-} cm^{-3} with an r^{-2} radial falloff removed by the analysis. The reconstruction shows that the primary portion of the CME dense material moves to the solar West as observed from the Earth with some of the material from these events present more than 180° from the Sun – Earth line. (b) The relative locations of Earth and Mars at this time as seen from directly above the ecliptic plane superimposed on an ecliptic cut of density extracted from the tomographic reconstruction also scaled in density as in (a).

value for the smaller peaks is just under 3 nPa for events just at the Mars event threshold of 3.5 nPa for both time-dependent and corotating models. Assuming that the associations of peaks in the *Mars Global Surveyor* analyses and the peaks in the IPS modeling analyses are accurate, this indicates that the IPS modeling gives ram pressures that are slightly lower (by about 85%) than those observed by *Mars Global Surveyor*; that is, the IPS modeling predicts a lower bulk density, a lower velocity, or both. Because the *Mars Global Surveyor* proxy does not account for all terms in the pressure balance, this slightly lower limit on the solar-wind ram pressure indicates that these unaccounted for terms must be rather minor contributions to the Mars magnetospheric solar-wind pressure.

The time-dependent 3D reconstruction is expected to primarily show transient events, and in the interval of study from 1999 to 2004, these are mostly CME-associated events. Although a time lag of zero days is the most frequent time lag for the time-dependent model, there are also time lags with a peak in the correlation above the noise level that are as distant as two days from the expected event time. In addition, there is a slight tendency for these time-dependent IPS-derived peaks to lag the *in situ* response seen by the *Mars Global Surveyor*. A two-day shift in the event time for the fastest CMEs is near the limit of what one would expect even though the model reconstructs a 3D structure that can miss Mars in both time and spatial dimensions and that may not model CME deceleration accurately (see the following). Clearly, the CME shape is not very accurately given since the IPS time-dependent model resolution is only 20° × 20° in latitude and longitude with a one-day temporal cadence, and the IPS measurements are obtained from sources that maximize their

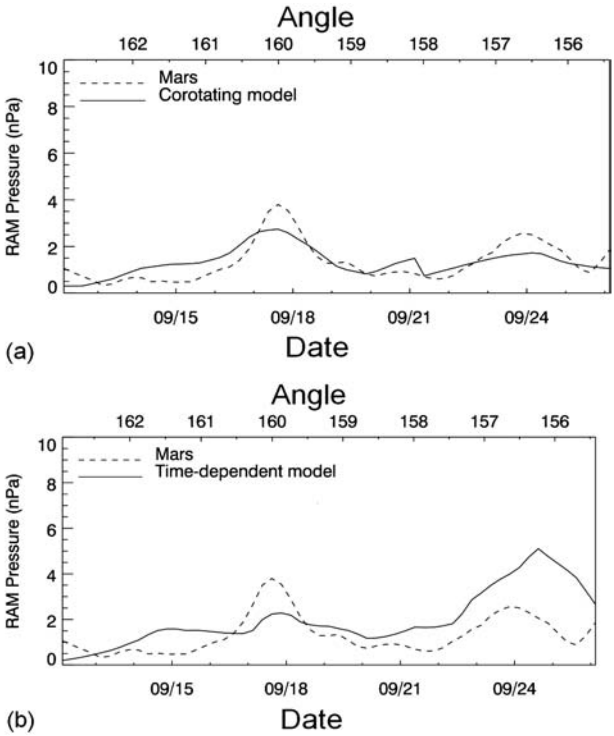

Figure 4 Mars time-series pressure analysis for the time period from 12 to 26 September 2002, associated with a series of CME events that occurred several days earlier. The Mars *in situ* response to the events begins about midway through 15 September and continues for several days. The angle of Mars west of the Sun – Earth line is given at the top of each time series. The only peak in the *Mars Global Surveyor* pressure above the 3.5 nPa criterion within this time interval occurred on 17 September. (a) Corotating model. (b) Time-dependent model.

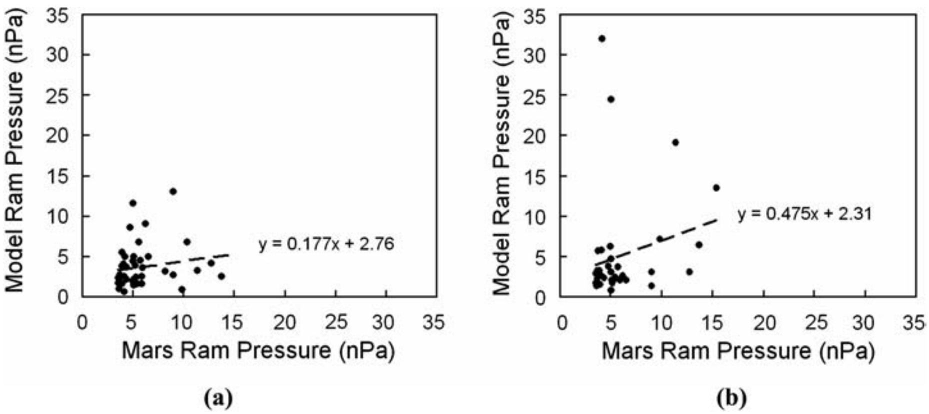

Figure 5 Comparison between the ram pressure peak amplitude at Mars from the *Mars Global Surveyor* and the IPS reconstructions for (a) 42 events for the corotating model and (b) 37 events for the time-dependent model.

response at about 0.5 AU from the Sun (Jackson *et al.*, 1998). Regardless, CME events with speed near 1000 km s^{-1} should generally appear at Mars in the 3D reconstructions and in the *in situ* response seen by *Mars Global Surveyor* within one day of each other. We do not know the reason for this apparent slight discrepancy, if it is real. In speculation however, we note that there are often fast forward shocks that accompany fast CMEs and these often are

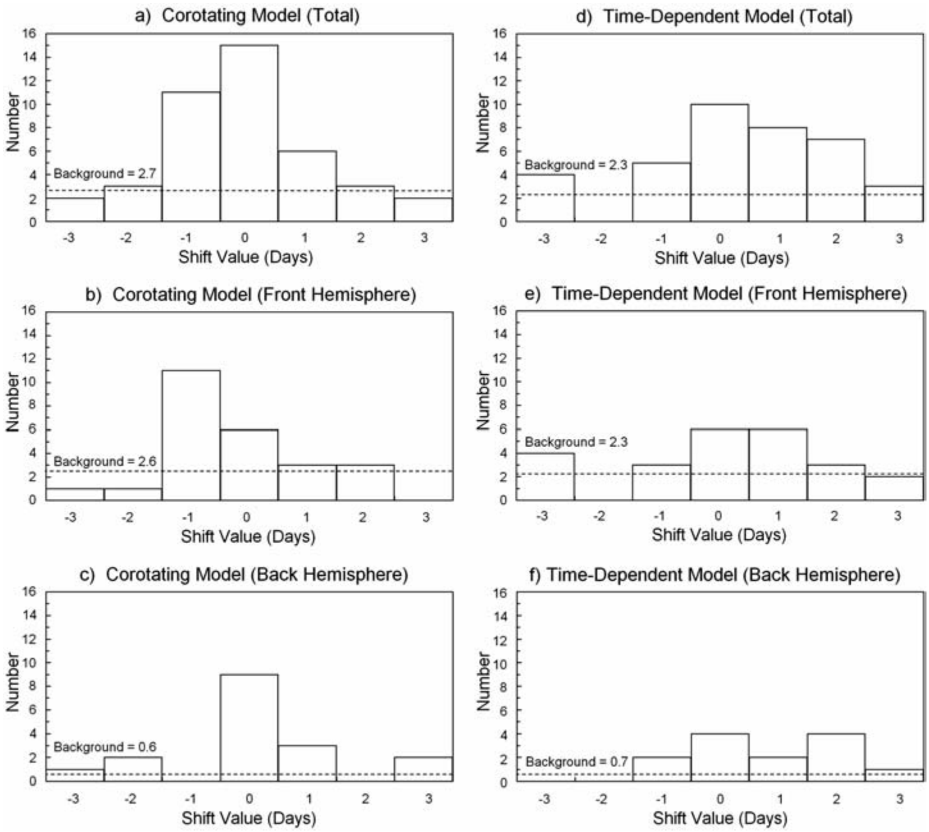

Figure 6 Histograms of the time lags between ram-pressure peaks observed at Mars by the *Mars Global Surveyor* with the peaks observed in the corotating and time-dependent IPS models. A positive shift indicates a lag in the IPS model relative to the *Mars Global Surveyor* data, and a negative shift indicates a lead in the IPS model relative to the *Mars Global Surveyor* data. (a) – (c) give, respectively, the numbers of corotating total events, the Sun-toward-Earth events, and the Sun-away-from-Earth events. (d) – (f) give, respectively, the numbers of time-dependent total events, the Sun-toward-Earth events, and the Sun-away-from-Earth events.

associated with a large response at the Earth's magnetosphere. The IPS kinematic modeling assumptions contain no mechanism to produce a shock response in our analyses. From the Bastille Day CME (Jackson and Hick, 2004), and from other fast CME measurements where the modeled shock response is not well observed in our analyses, we suppose that it is possible that the lag in the time-dependent model from the response at Mars could possibly be from an inadequate shock mechanism in our kinematic model. As a result, we would expect the IPS modeling to generally underestimate the propagation velocity of the CME and hence generally overestimate the CME response travel time from Sun to Mars. This may explain, in part, the tendency for some IPS events at Mars to lag the *in situ* peak in the *Mars Global Surveyor* analyses. In addition, there are surely some event misidentifications in our sample. Often several CMEs leave the active Sun within days of each other, and these events may not appear as individual events at Mars nor can they be clearly separated in our current low-resolution time-dependent IPS modeling, especially the smaller events.

The corotating reconstruction shows primarily corotating solar features, with twice the spatial resolution in solar longitude to approximately a two-thirds day arrival discrepancy. However, during periods of high solar activity it is clearly a mistake to claim solar-wind features are corotating, especially in terms of density; clearly an ensemble of transient effects produces an average of features appearing to corotate associated with a given solar activity center. Thus, the histograms of Figures 6a–c in comparison with those of Figures 6d–f show that indeed regions of corotating high density and velocity during this period are at least partly made up of transient events, and that these extend in time over perhaps as many as several days.

We have presented results of the IPS 3D reconstruction techniques in a comparison with *in situ* solar-wind ram-pressure analyses at Mars from the *Mars Global Surveyor*. As our models become more sophisticated, such as by using a 3D-MHD kernel in the tomographic analysis, we expect the comparisons to improve. In addition, we also expect to soon provide a similar result with the much higher resolution 3D reconstructions made possible using SMEI Thomson-scattering density modeling. This study does not specifically address the forecast capability of this technique as demonstrated with our near-real-time analyses of the IPS data. However, these same modeling techniques provide a forecast of solar-wind conditions at Mars when the IPS arrays are operating, and thus they have the potential to provide a forecast of solar-wind conditions at Mars several days in advance. No spacecraft at Mars currently monitors solar-wind velocity and density regularly. When *in situ* solar-wind monitoring instruments are present on spacecraft near Mars, comparisons with the IPS and/or SMEI 3D reconstructions should become even more relevant and precise.

Acknowledgements B.V. Jackson, J.A. Boyer, P.P. Hick, A. Buffington, and M.M. Bisi were supported at the University of California at San Diego by NSF Grant No. ATM-0331513; by NASA Grant Nos. NAG5-13453, NNG05GM58G, and NAG5-11906; and by AFOSR MURI Grant No. SA3213 subcontract to the University of California at Berkeley. D.H. Crider was supported at the Catholic University of America by NASA Grant Nos. NAG5-11225 and NAG5-12235. The authors wish to acknowledge and thank the group at STELab, Nagoya University (M. Kojima, M. Tokumaru, K. Fujiki, and students), for their continued support and for making IPS data sets available under the auspices of a joint collaborative agreement between the Center for Astrophysics and Space Sciences at UCSD and STELab.

References

Ananthakrishnan, S., Coles, W.A., Kaufman, J.J.: 1980, *J. Geophys. Res.* **85**, 6025.

Behannon, K.W., Burlaga, L.F., Hewish, A.: 1991, *J. Geophys. Res.* **96**(21), 213.

Brain, D.A., Halekas, J.S., Lillis, R., Mitchell, D.L., Lin, R.P., Crider, D.H.: 2005, *Geophys. Res. Lett.* **32**, L18203.

Crider, D.H., Vignes, D., Krymskii, A.M., Breus, T.K., Ness, N.F., Mitchell, D.L., Slavin, J.A., Acuña, M.H.: 2003, *J. Geophys. Res.* **108**(A12), 1461.

Crider, D.H., Espley, J., Brain, D.A., Mitchel, D.L., Connerney, J.E., Acuna, M.H.: 2005, *J. Geophys. Res.* **110**(A9), A09S21.

Dunn, T., Jackson, B.V., Hick, P.P., Buffington, A., Zhao, X.P.: 2005, *Solar Phys.* **227**, 339.

Eyles, C.J., Simnett, G.M., Cooke, M.P., Jackson, B.V., Buffington, A., Hick, P.P., Waltham, N.R., King, J.M., Anderson, P.A., Holladay, P.E.: 2003, *Solar Phys.* **217**, 319.

Gapper, G.R., Hewish, A., Purvis, A., Duffett-Smith, P.J.: 1982, *Nature* **296**, 633.

Hewish, A., Bravo, S.: 1986, *Solar Phys.* **106**, 185.

Hewish, A., Scott, P.F., Wills, D.: 1964, *Nature* **203**, 1214.

Hick, P.P., Jackson, B.V.: 2003, In: *Proc. SPIE* **5171**, 287.

Hildner, E., Gosling, J.T., MacQueen, R.M., Munro, R.H., Poland, A.I., Ross, C.I.: 1975, *Solar Phys.* **42**, 163.

Houminer, Z.: 1971, *Nature Phys. Sci.* **231**, 165.

Jackson, B.V., Hick, P.P.: 2004, In: Gary, D.G., Keller, C.U. (eds.) *Solar and Space Weather Radiophysics: Current Status and Future Developments*, *Astrophysics and Space Science Library* **314**, Kluwer, Dordrecht, 355.

Jackson, B.V., Hick, P.L., Kojima, M., Yokobe, A.: 1998, *J. Geophys. Res.* **103**, 12 049.

Jackson, B.V., Hick, P.P., Buffington, A.: 2002, In: *Proc. SPIE* **4853**, 23.

Jackson, B.V., Hick, P.P., Buffington, A., Kojima, M., Tokumaru, M., Fujiki, K., Ohmi, T., Yamashita, M.: 2003, In: Velli, M., Bruno, R., Malara, F. (eds.) *Proc. Solar Wind X, AIP Conf. Proc.* **679**, 75.

Jackson, B.V., Buffington, A., Hick, P.P., Altrock, R.C., Figueroa, S., Holladay, P.E., Johnston, J.C., Kahler, S.W., Mozer, J.B., Price, S., Radick, R.R., Sagalyn, R., Sinclair, D., Simnett, G.M., Eyles, C.J., Cooke, M.P., Tappin, S.J., Kuchar, T., Mizumo, D., Webb, D.F., Anderson, P.A., Keil, S.L., Gold, R.E., Waltham, N.R.: 2005, *Solar Phys.* **225**, 177.

Jackson, B.V., Buffington, A., Hick, P.P., Wang, X., Webb, D.: 2006, *J. Geophys. Res.* **111**, A04S91.

Kojima, M., Kakinuma, T.: 1987, *J. Geophys. Res.* **92**, 7269.

Tokumaru, M., Kojima, M., Fujiki, K., Yamashita, M., Jackson, B.: 2005, In: *Presentation at the XXVIII General Assembly of International Union of Radio Science (URSI), New Delhi, October 23 – 29*.

Tokumaru, M., Kojima, M., Fujiki, K., Yamashita, M., Jackson, B.V.: 2007, in press. doi: 10.1029/2006JA012043.

Vennerstrom, S., Olsen, N., Purucker, M., Acuña, M.H., Cain, J.C.: 2003, *Geophys. Res. Lett.* **30**, 1369.

Verigin, M., Vignes, D., Crider, D., Slavin, J., Acuña, M., Kotova, G., Remizov, A.: 2004, *Adv. Space Res.* **33**, 2222.